Original Article

Positive visualization of MR-compatible nitinol stent using a susceptibility-based imaging technique

Caiyun Shi[1], Guoxi Xie[2,3], Dong Liang[1], Haifeng Wang[1], Yi Huang[4], Yanan Ren[5], Yong Xue[4], Hanwei Chen[4], Shi Su[1], Xin Liu[1]

[1]Shenzhen Key Laboratory for MRI, Lauterbur Research Center for Biomedical Imaging, Shenzhen Institutes of Advanced Technology, Chinese Academy of Sciences, Shenzhen 518055, China; [2]Department of Radiology, The Six Affiliated Hospital, Guangzhou Medical University, Qingyuan 511518, China; [3]Department of Biomedical Engineering, Guangzhou Medical University, Guangzhou 511436, China; [4]Department of Radiology, Guangzhou Panyu Central Hospital, Guangzhou 511400, China; [5]Department of Magnetic Resonance Imaging, The First Affiliated Hospital of Zhengzhou University, Zhengzhou 450052, China

Correspondence to: Guoxi Xie. Department of Biomedical Engineering, Guangzhou Medical University, Guangzhou 511436, China. Email: guoxixie@163.com.

Background: MR-compatible metallic stents have been widely used for the treatment of arterial occlusive diseases. However, conventional MR techniques have difficulty in accurately localizing the stent position and access the stent restenosis because of the susceptibility and radiofrequency (RF) shielding artifacts caused by the stent mesh. Previous studies have demonstrated that a susceptibility-based positive contrast MR method exhibits excellent efficacy for visualizing MR compatible metal devices. However, the method had not been evaluated in the visualization of stents and for the assessment of stent restenosis.

Methods: The susceptibility-based positive contrast MR method was used to visualize the nitinol stents and assess the stent restenosis by comparing two typical MR positive contrast techniques, i.e., susceptibility gradient mapping using the original resolution (SUMO) and the gradient echo acquisition for super-paramagnetic particles (GRASP) with positive contrast.

Results: Three sets of experiments were respectively performed to investigate the influence of stent orientation and spatial resolution on the susceptibility-based method, and to demonstrate the feasibility of the susceptibility-based method in evaluating the stent restenosis comparing to the two typical MR positive contrast methods, GRASP and SUMO.

Conclusions: The susceptibility-based method provides better visualization and localization of the stent than SUMO and GRASP and has the capability of assessing the stent restenosis.

Keywords: Positive contrast; magnetic resonance imaging; susceptibility; stent; stent restenosis

Submitted Aug 09, 2018. Accepted for publication Nov 09, 2018.
doi: 10.21037/qims.2019.03.15
View this article at: http://dx.doi.org/10.21037/qims.2019.03.15

Introduction

MR-compatible metallic implanted devices, such as the endovascular stent grafts, are commonly used for the treatment of arterial occlusive diseases (1). Computed tomography (CT) is currently the standard imaging modality to assess the stent restenosis and localize the metallic implanted devices (2). In addition, the improved computed tomography technique, such as synchrotron radiation computed tomography (3), allows for a more accurate assessment of the stent and size measurement of different aortic stent grafts. The dual energy computed tomography angiography (DECTA) which can obtain better image quality in peripheral arterial stenting when compared to conventional CTA (4). However, CT requires exposure to ionizing radiation and has limited soft tissue contrast (5-8). In recent years, several MR techniques have

been proposed for scanning the patients with implanted MR compatible stent because of their superior soft tissue contrast. MR angiography (MRA) and contrast-enhanced MRA techniques are respectively proposed by some scholars to image MR compatible metallic stents (9-11) non-invasively. The results show that intraluminal loss of signal and artifacts of most of the SFA (superficial femoral artery) stents do not markedly limit assessment of stent lumen by MRA at 1.5 and 3T. MRA can be considered a valid technique for the detection of relevant in-stent restenosis. Furthermore, the inversion recovery with on-resonant water suppression (IRON) with conventional T1-weighted (T1w) MRA is proposed for visualization of peripheral nitinol stents (12). IRON-MRA provides an improvement of the in-stent lumen visualization with an 'open-close-open' design, which reveals a complete in-stent signal loss in T1W MRA. However, the fat-saturated T2-weighted imaging can limit assessment of in-stent pathology of the cobalt-chromium stents because of the metal artifact (13). Additionally, these conventional MR techniques neither accurately localize the position of the implanted devices nor assess the stent restenosis due to the susceptibility and radiofrequency (RF) shielding artifacts caused by the stent graft. Therefore, a reliable MR technique for visualizing the metallic devices and assessing the stent restenosis would be highly beneficial.

Two existing MR-positive contrast techniques have the potential for the visualization of superparamagnetic particles or metallic devices but have not yet been used for the stent restenosis assessment. One technique, gradient echo acquisition for superparamagnetic particles (GRASP), applies to a decreased rephasing gradient for slice selection. This technique compensates for the susceptibility gradients along the slice direction and is sensitive to magnetic field inhomogeneities (14,15). Another technique, susceptibility gradient mapping (SGM), uses the conventional gradient echo sequence for data acquisition and apples a short-term Fourier transform over a small window (16) to generate the positive contrast MR images. Also, an improved version of SGM using the original resolution (SUMO) employs a truncated filter in k-space instead of the short-term Fourier transform to maintain the original image resolution (17). However, both SGM and SUMO are based on the phase of field perturbation which spreads out from the metallic devices. Thus, the positive contrast regions obtained by SGM and SUMO are extended which only highlight the surrounding area of the metallic devices (17-19).

Recent studies demonstrate that a susceptibility-based positive contrast MR method exhibits excellent efficacy for visualizing MR compatible metal devices (i.e., biopsy needle and brachytherapy seeds) by taking advantage of their high magnetic susceptibility and the sparsity of the positive contrast MR images (20,21). However, the method was not evaluated for the visualization of stents and stent restenosis. Therefore, the purpose of this study was to prospectively evaluate whether the susceptibility-based method can be used to visualize the nitinol stents and assess the stent restenosis, as well as to compare it with the SUMO and GRASP methods.

Susceptibility-based positive contrast method

This method employs a modified 2D fast spin echo (FSE) sequence to accelerate data acquisition (21). The technique uses an equivalent short echo time (TE) by shifting the readout gradient by T_{shift} during MR data acquisition. Two datasets with and without readout shifts (T_{shift} in the range of 0.2–0.7 ms) are acquired for measuring the field induced by MR-compatible metallic devices. Thus, the extent of phase change induced by the local susceptibility difference between the metallic devices and the surrounding tissues is accumulated during T_{shift}. After data acquisition, a kernel deconvolution algorithm with a regularized $\ell 1$ minimization is used to calculate the susceptibility mapping and acquire positive contrast images. As the stents have much higher susceptibility values than the surrounding tissues, the susceptibility-based technique can visualize the metallic devices in positive contrast. Furthermore, the technique may be used to assess the stent restenosis because the materials and the surrounding tissues have different susceptibilities and therefore manifest a different contrast in the susceptibility map.

SUMO

An object with a magnetic susceptibility that deviates from its surrounding creates a local inhomogeneous magnetic field. The local susceptibility gradient G^{susp} can be considered as an additional gradient overlapped on the imaging gradients G^{img}, which leads to an echo-shift in k-space for the signal that stems from the affected voxel (16). G^{susp} for a given voxel is proportional to the echo-shift $m_{x,y,z}$ in k-space:

$$G^{susp}_{x,y,z} \approx -\frac{m_{x,y,z} G^{img}_{x,y,z} \tau_{x,y,z}}{TE} \quad [1]$$

where $\tau_{x,y,z}$ represents the duration of the imaging gradient. A modified k-space filter can be applied in k-space to get the echo-shift $m_{x,y,z,}$ and the positive-contrast image is then generated by a map of the strength of the susceptibility-gradient vector G^{susp} (17).

GRASP

GRASP is a technique that employs a modified 2D gradient echo sequence to obtain a positive contrast image (14). In a conventional gradient echo acquisition, the slice selection gradient dephases the spins after an excitation pulse. To rephase the excited spins, usually the full 100% rephasing gradient is used to compensate for the slice selection area. This is indicated by the magnetic moment of zero at the completion of the rephasing gradient pulse. If the amplitude of this rephasing gradient is decreased (for example, to 50%), it creates a gradient imbalance effectively reducing the signal under normal circumstances. However, in locations where a negative local gradient caused by an MR-compatible metallic device is present, the gradient balance is restored, and a bright signal can be seen. The signal is conserved in the region near the metallic devices because the induced dipole field compensates for the rephasing gradient. Therefore, a hyperintense signal is observed near the metallic devices against the dark background.

Methods

Data acquisition

To evaluate whether the susceptibility-based method can be used to visualize the stent, three sets of experimental data were acquired by the modified FSE sequence on a 3T whole-body MRI scanner (Siemens Tim Trio, Germany) with an eight-channel phased array coil. The experiments were carried out with a tracheal stent [Micro-Tech (Nanjing) Co., Ltd.] in which the direction of the stent was parallel to the axis of the cylindrical phantom doped with 1.0 g/L copper sulfate solution. The stent was made with 0.24 mm diameter Ni-Ti alloy wire (magnetic susceptibility $\chi_{nitinol}$ =245 ppm) and the size of the stent was length × diameter = 60 mm × 20 mm with a cylindrical shape.

The first experiment was designed to investigate the influence of stent orientation and spatial resolution on the susceptibility-based method. The phantom was positioned parallel to B_0 and datasets were obtained with the main axis of the stent orientated at 0°, 30°, 60°, and 90° relative to the main magnetic field, B_0. Scan parameters were: FOV = 128×128 mm^2, matrix size = 192×192, TR =2,000 ms, TE = 18 ms, slice number = 20, in-plane resolution = 0.67×0.67 mm^2, slice thickness =1.5 mm, slice gap =0.0 mm, bandwidth =134 Hz/Pixel, and T_{sbift} =0.6 ms. Total acquisition time was 3.16 minutes. Subsequently, for spatial resolution, the stent orientation was fixed to 0° relative to B_0 and MR data were acquired with a spatial resolution of 0.5×0.5, 0.7×0.7, and 1.0×1.0 mm^2. The other scan parameters were: FOV =128×128 mm^2, TR =2,000 ms, TE =18 ms, slice gap =0 mm, bandwidth =134 Hz/Pixel, and T_{sbift} =0.6 ms. Both axial and coronal multi-slice data were acquired using the modified FSE sequence without partial Fourier or parallel imaging. In the study, a turbo factor of 7 was chosen to provide a tradeoff between the signal-to-noise ratio (SNR) and imaging speed. In addition, the experiments with varying angles (0°, 30°, 60°, and 90°) between the stent's long axis and the main magnetic field B_0 for the SUMO and GRASP protocols were also executed for the comparison. For the SUMO technique, a 3D GRE sequence was used to collect data. Imaging parameters included: TR =6.2 ms, TE =2.5 ms, FA =15°, slice thickness =1.5 mm, and bandwidth =500 Hz/Pixel. For the GRASP technique, a modified 2D GRE sequence was used to collect data and the scan parameters included: TR =11.5 ms, TE =5 ms, slice thickness =2 mm, bandwidth =130 Hz/Pixel, and the gradient rephasing was previously optimized as 50% of that used in the ordinary GRE sequence. All two methods had the same in-plane spatial resolution of 0.67×0.67 mm^2 and slice/partition number was 20.

The second experiment was carried out to demonstrate the ability of the susceptibility-based method to visualize the nitinol stents comparing to the two typical MR positive contrast methods, GRASP and SUMO. The stent orientation was fixed to 0° relative to B_0. In the susceptibility-based method, two data sets were obtained with and without T_{sbift} of 0.6 ms using the modified 2D FSE sequence with the following scan parameters: TR =2,000 ms, TE = 18 ms, slice thickness =1.5 mm with no gap, and bandwidth =134 Hz/Pixel. For the SUMO and GRASP technique, the scan parameters were the same as experiment one.

The third experiment was performed to demonstrate the feasibility of the susceptibility-based method in evaluating the stent restenosis. The same Ni-Ti stent was used to simulate the stent restenosis, i.e., no stenosis, external stenosis, and internal stenosis by using the approach introduced by Nordmeyer (22). Specifically, *Figure 1A* was the phantom of descending thoracic pig aorta, the stent was

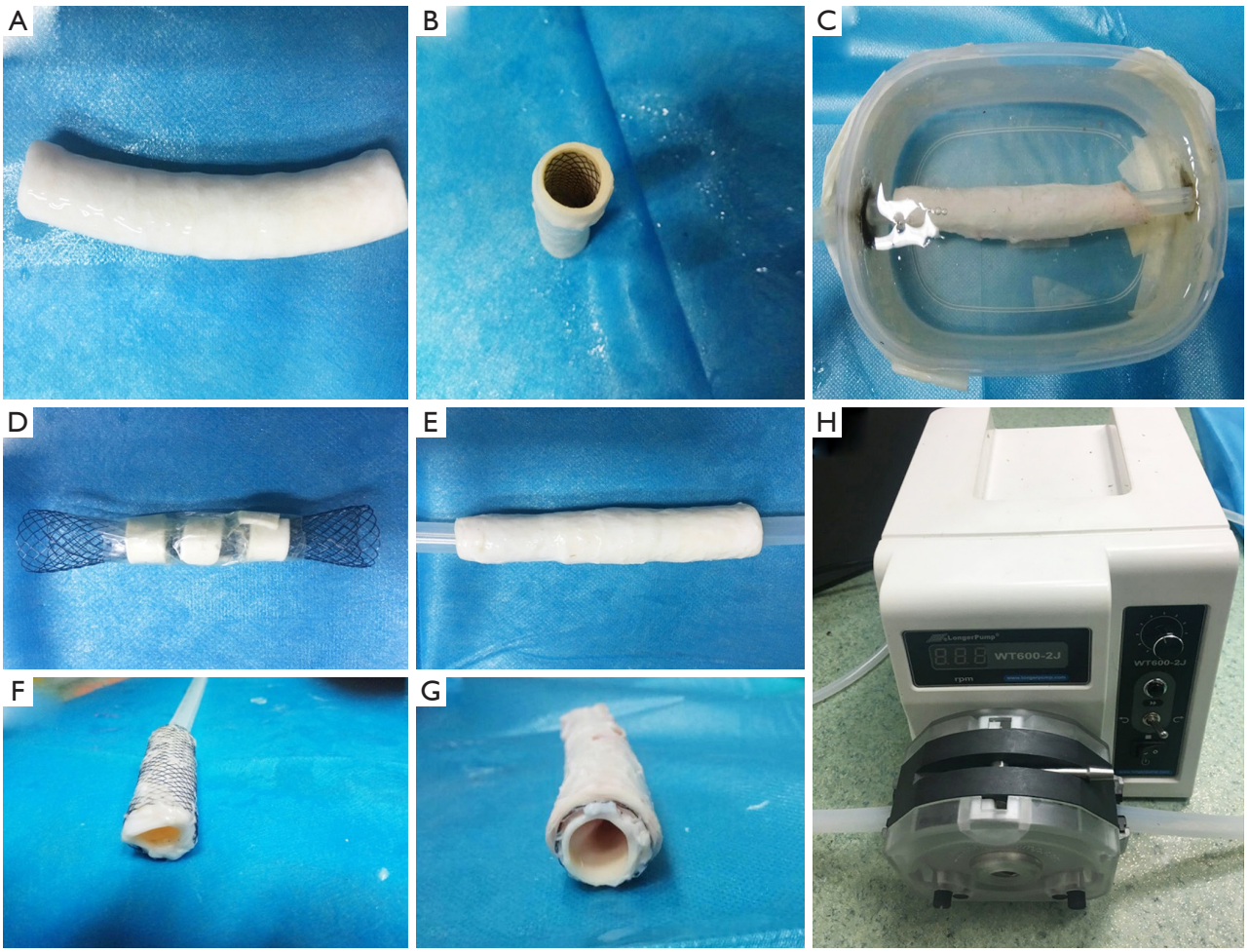

Figure 1 Experimental setup for the stent restenosis. (A) Phantom of descending thoracic pig aorta; (B) stent implanted into the descending thoracic pig aorta which was used to simulate the stent without stenosis; (C) the vessel phantom embedded in the methylcellulose-filled plastic container; (D) external stent stenosis (external stenosis) created by wrapping a plastic tie outside the stent; (E) the vessel phantom with external stenosis; (F) internal stent stenosis (internal stenosis) created by suturing aortic vessel material to the inner surface of the stent; (G) the vessel phantom with implanted internal stenosis; (H) the peristaltic pump (WT600, Longer pump, Shandong) used to drive the vessel phantoms.

implanted into a portion of excised descending thoracic pig aorta (length =100 mm and diameter =20–25 mm) which was used for simulating the stent without stenosis (*Figure 1B*), and the aorta model was housed in a methylcellulose-filled plastic container (*Figure 1C*). The orientation of the stent was positioned parallel to B_0. External stenosis was formed by wrapping a plastic tie around the stent implantation site (*Figure 1D*). So, the vessel phantom with external stenosis was formed after that the pig aorta was encased in the stenosis model D (*Figure 1E)*. Internal stenosis was fashioned by suturing aortic vessel material into the inner surface of the stent (*Figure 1F*). So, the vessel phantom with internal stenosis was formed after that the pig aorta was encased in the stenosis model F (*Figure 1G*). After preparing the aorta model, it was attached to a peristaltic pump (WT600, Longer pump, Shandong, China) with a combination of rigid and silicone tubes (*Figure 1H*). The pulsatile flow was approximately 5 L/min. A 40:60 solution of 87% glycerol and water was used to mimic the MRI (T1 =850 ms, T2 =170 ms) and viscous properties of blood (23). Then the stent restenosis phantom was imaged with susceptibility-based, SUMO, and GRASP methods. All images were obtained with the same 3T MR scanner, and the stent was positioned parallel to B0 field. In

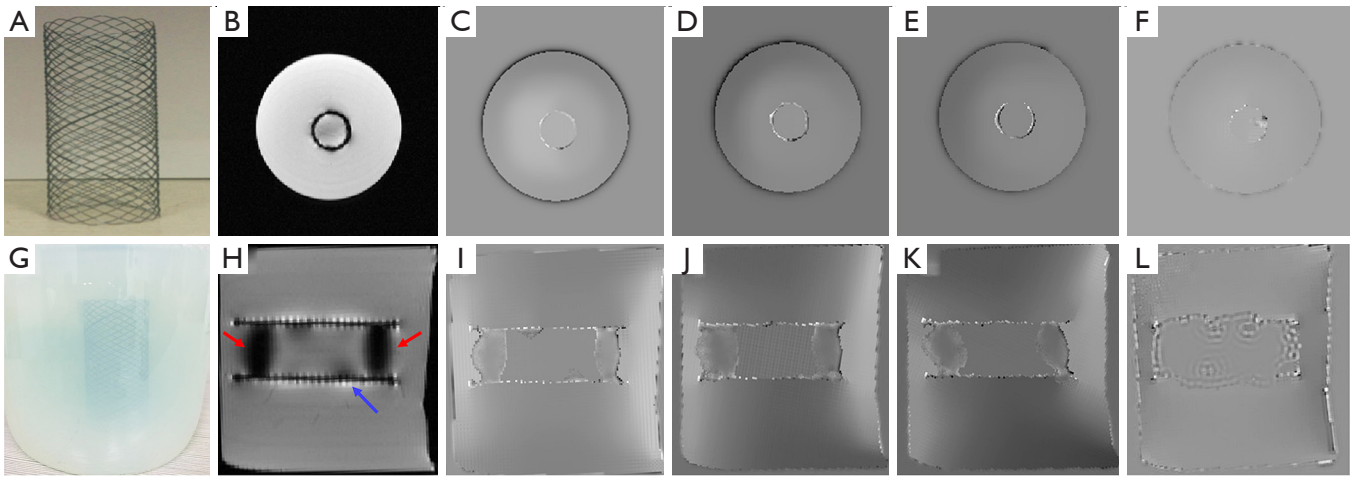

Figure 2 Positive contrast stent images from the proposed method. The stent was placed at different orientations relative to the main magnetic field (0°, 30°, 60°, and 90°). (A) The stent model; (C,D,E,F) the axial views; (G) the stent phantom; (I,J,K,L) the coronal views. Visualization of the stent is progressively worse at larger orientation angles because of the increasing effects of the susceptibility artifacts (blue arrow) and RF shielding artifacts (red arrows).

the susceptibility-based method, the same scan parameters were used as the second experiment. For the SUMO and GRASP techniques, image parameters were separately optimized. For the SUMO technique, a 3D GRE sequence was used to collect data. Scan parameters were: TR =19 ms, TE =2.5 ms, FA =15°, bandwidth =930 Hz/ Pixel, matrix size = 156×192×40, and in-plane spatial resolution =1.04×1.04×2.8 mm^3. For the GRASP technique, a modified 2D GRE sequence was used to collect data and the scan parameters included: TR =3,000 ms, TE =5 ms, matrix size =136×176×40, in-plane spatial resolution =0.9×0.9×4.0 mm^3, BW =130 Hz/Pixel, the gradient rephasing was respectively optimized as 40%, 60%, and 30% (no stenosis, external stenosis, and internal stenosis) of that used in the ordinary GRE sequence.

Image reconstruction and visualization

All data were processed offline, and the positive contrast images were reconstructed using the method in (20). The reconstructed positive-contrast images in the first two experiments were also overlaid onto the corresponding magnitude images for qualitative evaluation and comparison among the susceptibility-based method, SUMO, and GRASP. For quantitative analysis, the diameters of the stent were measured from the positive contrast images obtained by the three methods. For qualitative analysis of the third experiment, subjective assessment of the stent restenosis images was performed by two reviewers with several years of experience in cardiovascular imaging. The process of the experiment was conducted by the reviewers, who knew the true state of the stent. Finally, the imaging results were further analyzed, and post-processing techniques of the 3D MIP reconstructions for the stent restenosis (i.e., no stenosis, external stenosis, and internal stenosis) are conducted (Data from the third experiment).

Results

Figures 2-4 shows the positive contrast MR images of the stent with different orientations to B_0 using the susceptibility-based imaging method, SUMO and GRASP. *Figure 2B,H* display the representative axial and coronal magnitude images obtained by conventional FSE sequence (i.e., the modified FSE sequence without echo shifted). It is difficult to identify the accurate localization of the stent on the magnitude images due to the susceptibility artifacts (blue arrow) and RF shielding artifacts (red arrows). However, the location of the stent is highlighted on the corresponding positive contrast imaging (*Figure 2C,D,E,F,I,J,K,L*) where the orientation of the stent is 0°, 30°, 60°, and 90° related to B_0. As can be seen, the visualization of the stent is progressively worse with increasing decline angle of the B_0 field because of the mounting effects of the susceptibility artifacts and RF shielding artifacts. The best visualization is obtained at 0° as shown in *Figure 2C,I*. The results of

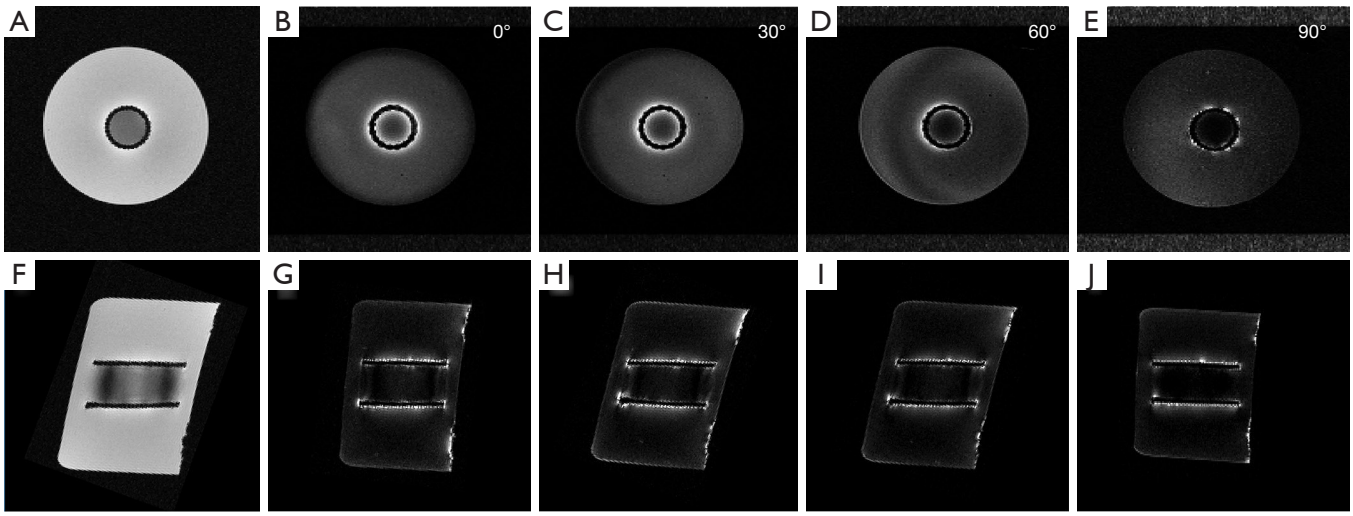

Figure 3 Positive contrast stent images from the SUMO. The stent was placed at different orientations relative to the main magnetic field (0°, 30°, 60°, and 90°). (A,F) Magnitude images; (B,C,D,E) the axial views; (G,H,I,J) the coronal views. Similar to the susceptibility-based method, visualization of the stent is progressively worse at larger orientation angles because of the increasing effects of the susceptibility artifacts. SUMO, susceptibility gradient mapping using the original resolution.

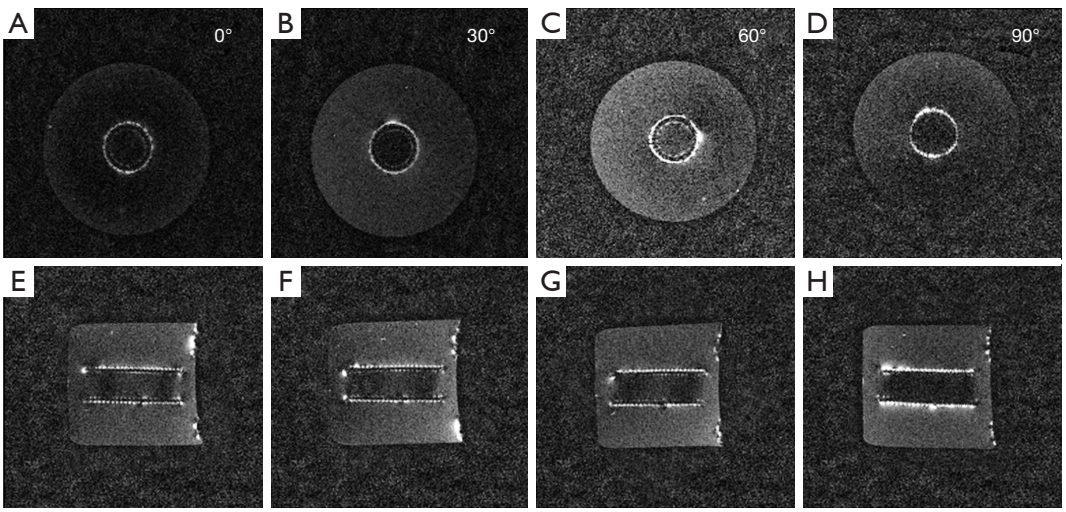

Figure 4 Positive contrast stent images from the GRASP method. The stent was placed at different orientations relative to the main magnetic field (0°, 30°, 60°, and 90°). (A,B,C,D) The axial views; (E,F,G,H) the coronal views. GRASP, gradient echo acquisition for super-paramagnetic particles.

the SUMO and GRASP (*Figures 3*,*4*) demonstrate that they have the same positive imaging performance as the susceptibility-based method. The visualization of the stent is also progressively worse at larger orientation angles because of the increasing effects of the susceptibility artifacts.

Figure 5 shows the positive visualization of the stent-graft using susceptibility-based imaging method at an in-plane resolution of 0.5, 0.7, and 1.0 mm. At 0.5 mm resolution, the stent has a lower contrast (*Figure 5A*,*D*). In contrast, the stent becomes less visible at 1.0 mm resolution (*Figure 5C*,*F*). The best visualization of the stent is obtained at the resolution of 0.7 mm on both the axial and coronal images.

Figures 6,7 show the results of the second experiment. As shown, all three methods successfully realize the

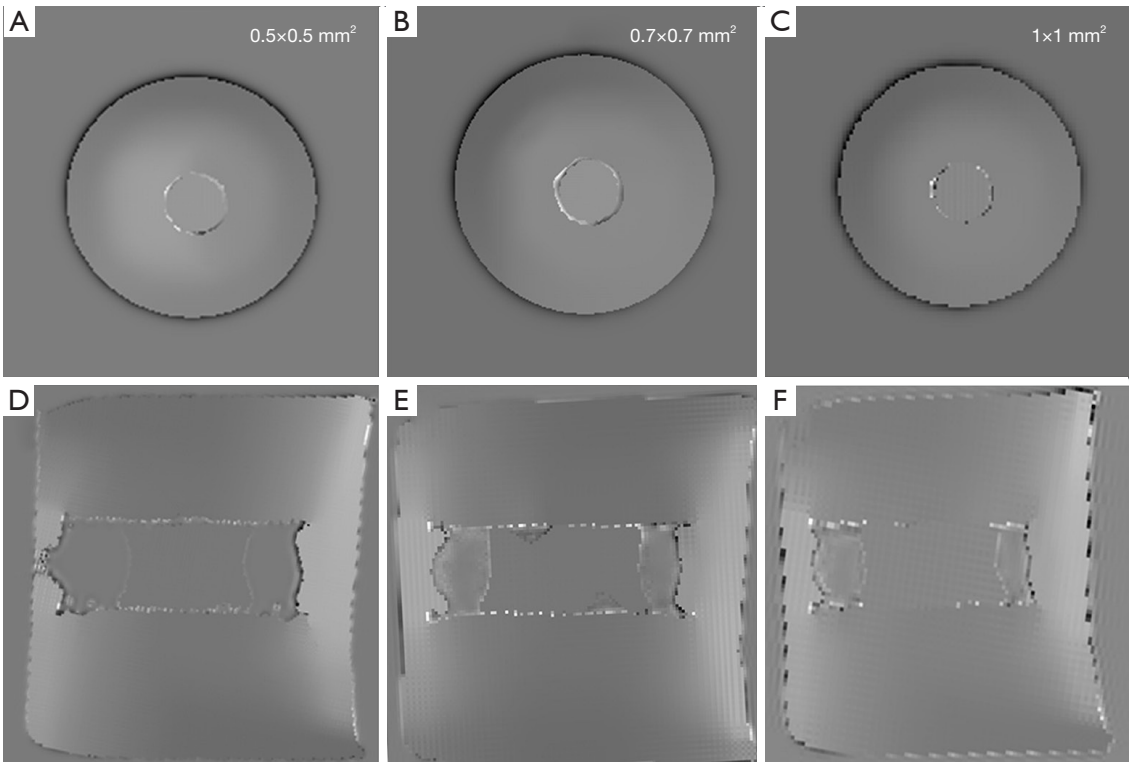

Figure 5 Positive contrast stent images from the proposed method at different planar resolution. There is a tradeoff between SNR and partial volume effect. The best stent visualization is obtained at the resolution of 0.7 mm in both the axial and coronal images. SNR, signal-to-noise ratio.

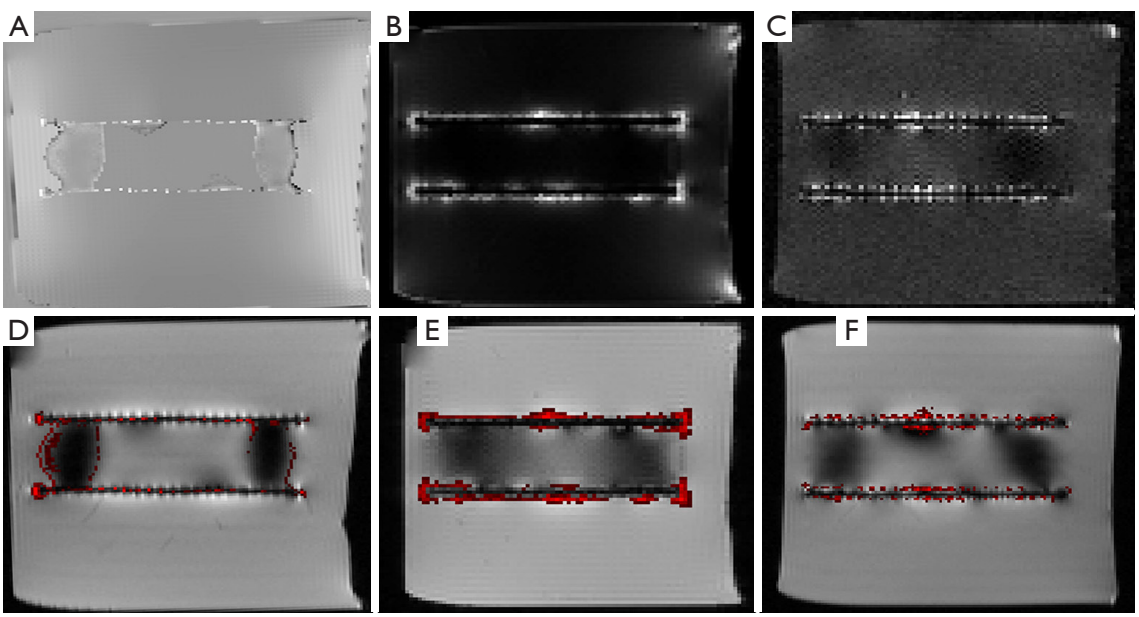

Figure 6 Coronal views of the positive contrast images of the stent phantom using (A) the susceptibility-based method, (B) SUMO, and (C) GRASP which are overlaid to their corresponding magnitude images (D,E,F). Compared to SUMO (E) and GRASP (F), the susceptibility-based method (D) allowed a more precise visualization of the stent location. SUMO, susceptibility gradient mapping using the original resolution; GRASP, gradient echo acquisition for super-paramagnetic particles.

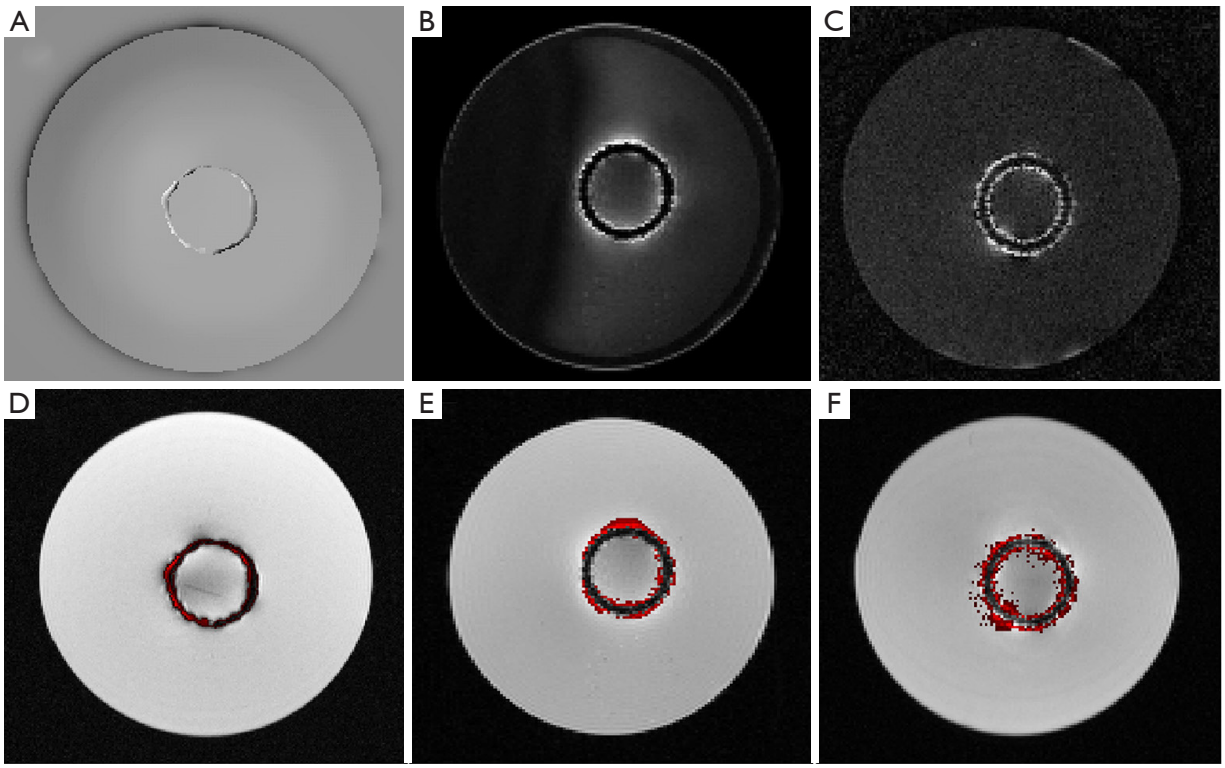

Figure 7 Axial views of positive contrast images of the stent phantom using (A) the susceptibility-based method, (B) SUMO, and (C) GRASP. The overlaid images also showed that the susceptibility-based method (D) provided better stent localization than SUMO (E) and GRASP (F). SUMO, susceptibility gradient mapping using the original resolution; GRASP, gradient echo acquisition for super-paramagnetic particles.

positive contrast imaging of the nitinol stent. Compared to SUMO (*Figures 6B*,*7B*) and GRASP (*Figures 6C*,*7C*), the susceptibility-based method (*Figures 6A*,*7A*) show the stent itself rather than its highlighted surrounding area with high susceptibilities. The susceptibility-based method can correctly localize the stent (*Figures 6D*,*7D)* which is demonstrated by the results of the positive contrast images overlaid onto the magnitude images. Better visualization of the stent is realized by the susceptibility-based method than by SUMO and GRASP according to the 3D MIP reconstruction (*Figure 8*).

According to the quantitative image analysis, the diameter of the stent measured by the susceptibility-based method is 20.2±0.8 mm, which is very close to the real one 20.0 mm (*Table 1*). However, the SUMO and GRASP methods highlight the surrounding area of the stent as two bright cycles in the corresponding positive contrast images. The average diameters, defined as (D1+D2)/2 in *Figure 9*, are both close to the real diameter (*Table 1*).

Representative images of the stent restenosis are shown in *Figures 10-12*. In all three images, the green arrows indicate the position of the vessel wall of the thoracic pig aorta, and the blue arrows indicate the position of the stent and the red arrows indicate restenosis. *Figure 10* exhibits the vessel imaging with no stenosis. The stent is dark shown by the conventional FSE (*Figure 10A*) but highlighted by the susceptibility-based method (*Figure 10B*), SUMO (*Figure 10C*), and GRASP (*Figure 10D*). *Figure 11* displays the vessel images of external stenosis. *Figure 12* shows the vessel images of internal stenosis. The post-processing techniques of 3D MIP reconstruction for the stent restenosis (i.e., no stenosis, external stenosis, and internal stenosis) are showed in *Figures 13-15*. All three positive contrast techniques mentioned above can provide good visualization of the stent lumen (*Figure 13*). However, the susceptibility-based method and the GRASP method has superior performance in the diagnostic accuracy of the external stenosis than SUMO (*Figure 14*). Furthermore, the susceptibility-based method and SUMO can provide a better diagnostic accuracy of the internal stenosis than

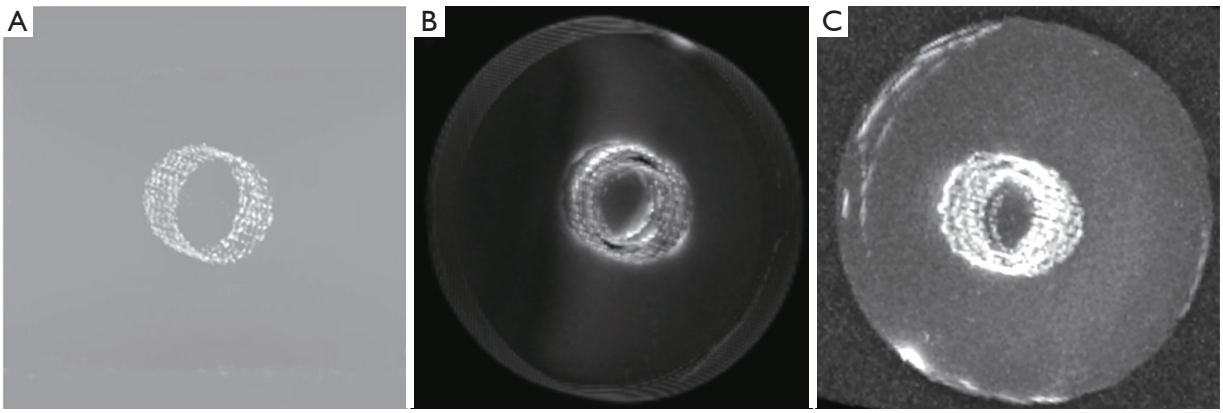

Figure 8 MIP reconstructions from the positive contrast images obtained by (A) the susceptibility-based method, (B) SUMO, and (C) GRASP. The susceptibility-based method provided a clear visualization of the stent. MIP, maximum intensity projection; SUMO, susceptibility gradient mapping using the original resolution; GRASP, gradient echo acquisition for super-paramagnetic particles.

Table 1 Diameter of the stent measured on the positive contrast images obtained by the susceptibility-based method, SUMO, and GRASP

Imaging method	Inner diameter (D1) (mm)	Outer diameter (D2) (mm)	Average diameter (mm)
The susceptibility-based method	–	–	20.2±0.8
SUMO	15.6±1.1	26.4±1.4	21.0±1.3
GRASP	17.8±1.5	23.9±1.7	20.9±1.6

The diameter obtained by the susceptibility-based method was very close to the real one 20.0 mm. SUMO, susceptibility gradient mapping using the original resolution; GRASP, gradient echo acquisition for super-paramagnetic particles.

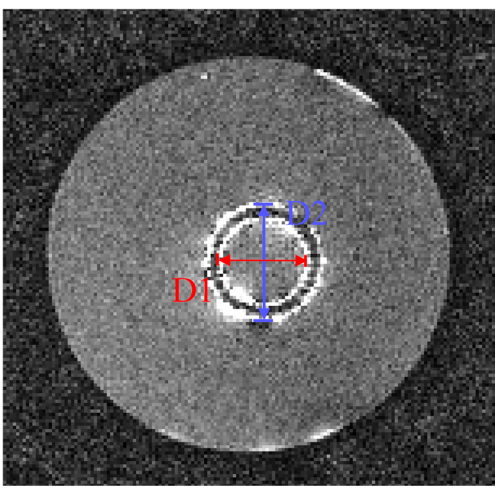

Figure 9 Illustration of the inner and outer diameters of the bright cycles on the stent which were obtained by GRASP and SUMO. The average diameter was obtained by (D1+D2)/2. GRASP, gradient echo acquisition for super-paramagnetic particles; SUMO, susceptibility gradient mapping using the original resolution.

the GRASP method (*Figure 1S*). Therefore, the proposed susceptibility-based method provides an excellent delineation of the stent lumen and different stenosis.

Discussion

It is well recognized that the presence of metallic stents can lead to severe RF shield and susceptibility artifacts limiting the utility of the conventional MR technique. In this study, we use a positive contrast MR technique, a susceptibility-based method, to directly visualize the stent and evaluate the inner and outer stenosis. Phantom results demonstrate that the method has the capability to localize the stent and identify stenosis and is superior to the other two positive contrast techniques (i.e., GRASP and SUMO) as well as the conventional FSE sequence.

Both stent orientation and voxel size can affect the visualization of the metallic device using the susceptibility-based method. In general, cylindrically shaped objects, such as stents, show the smallest susceptibility when positioned along the direction of the main magnetic field B_0 (24,25). Therefore, the nitinol wire frame is clearly depicted when it is placed parallel to B_0. However, visualization of the stent is progressively worse at larger orientation angles due to the increasing effects of the susceptibility artifacts and RF shielding artifacts. Even so, good visualization of the stent

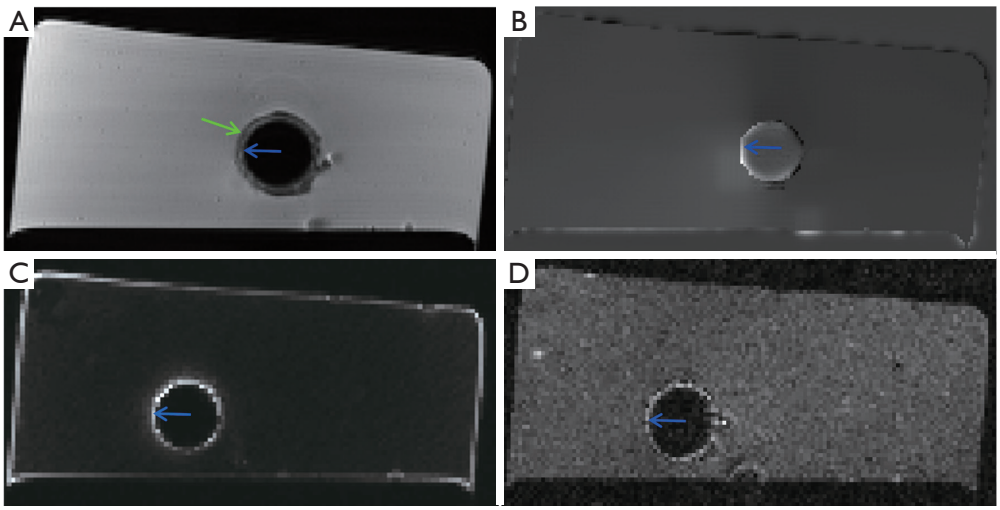

Figure 10 Representative images of the stent without stenosis obtained by (A) the conventional FSE, (B) the susceptibility-based method, (C) SUMO, and (D) GRASP. The green arrow points to the position of the vessel wall of the thoracic pig aorta, and the blue arrows point to the approximate position of the stent. SUMO, susceptibility gradient mapping using the original resolution; GRASP, gradient echo acquisition for super-paramagnetic particles.

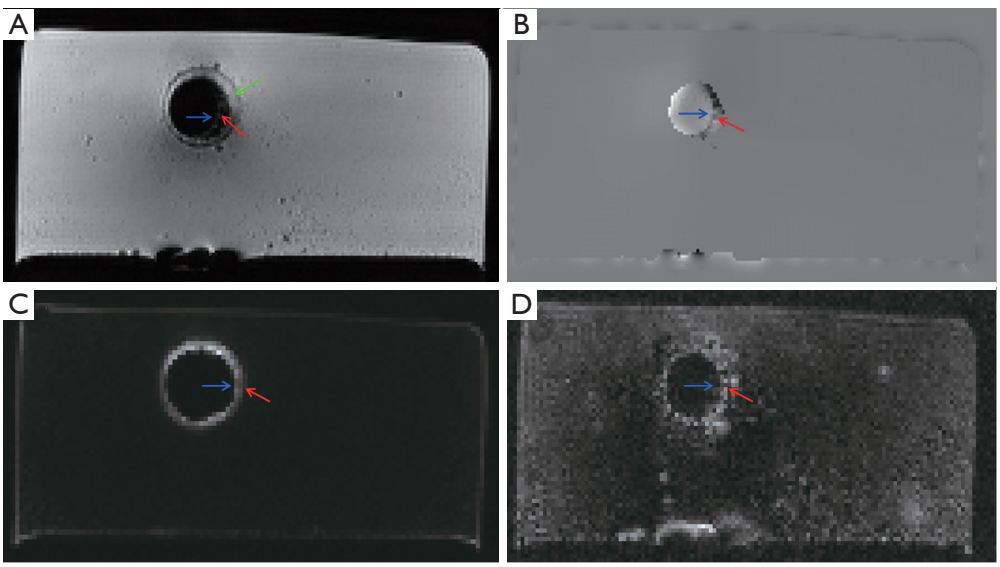

Figure 11 Representative images of the stent with external stenosis obtained by (A) the conventional FSE, (B) the susceptibility-based method, (C) SUMO, and (D) GRASP. The green arrow points to the position of the vessel wall of the thoracic pig aorta, the red arrows point to the external stenosis, and the blue arrows point to the approximate position of the stent. SUMO, susceptibility gradient mapping using the original resolution; GRASP, gradient echo acquisition for super-paramagnetic particles.

can be obtained under the 60° orientation relative to the main magnetic field. In addition, preliminary results also show that the nitinol stent can be visualized with the proposed method at up to 1 mm in-plane resolution. The contrast of the stent becomes smaller at higher spatial resolution because of the decreased SNR (*Figure 5A*,*D*). This is because the susceptibility-based method relies on signals with sufficient SNR from the surrounding areas of the implant devices

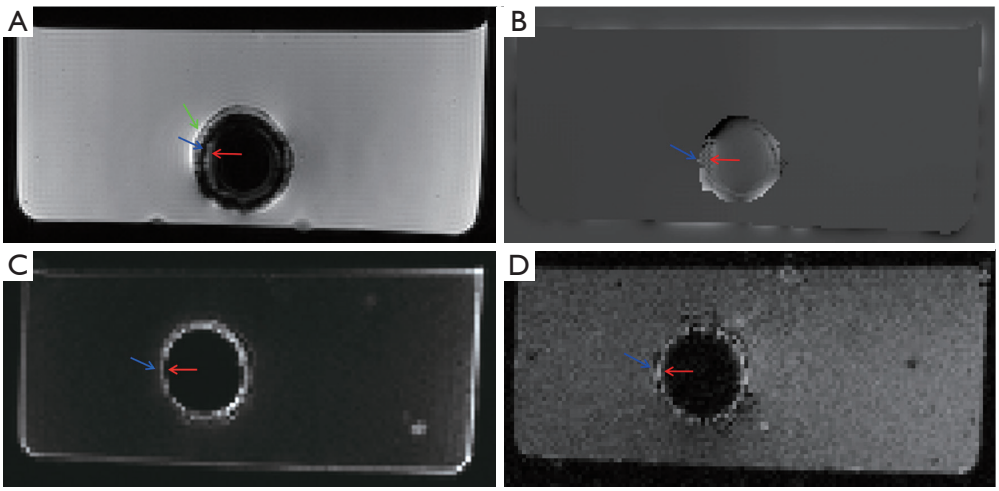

Figure 12 Representative images of the stent with internal stenosis obtained by (A) the conventional FSE, (B) the susceptibility-based method, (C) SUMO, and (D) GRASP. The green arrow points to the position of the vessel wall of the thoracic pig aorta, the blue arrows point to the position of the stent, and the red arrows indicate the internal stenosis. FSE, fast spin echo; SUMO, susceptibility gradient mapping using the original resolution; GRASP, gradient echo acquisition for super-paramagnetic particles.

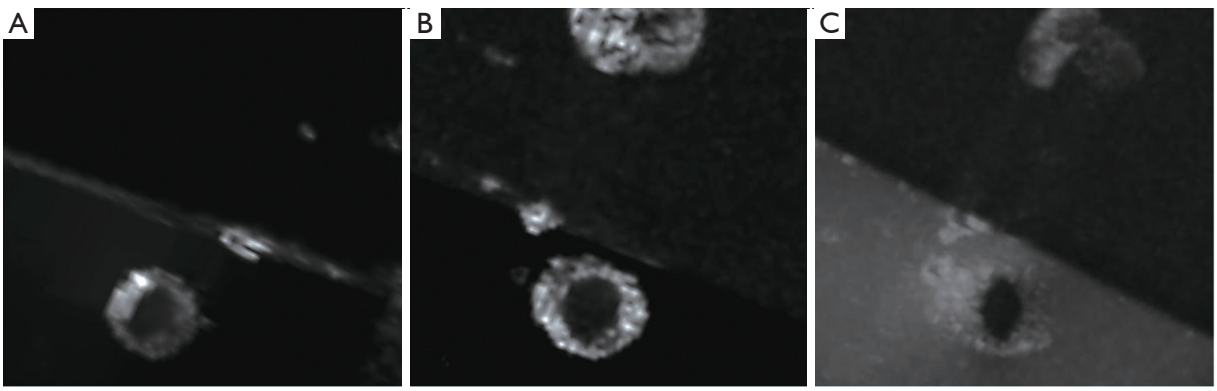

Figure 13 MIP reconstructions of the stent without stenosis (A) the susceptibility-based method, (B) SUMO, and (C) GRASP. The susceptibility-based method and the SUMO can provide a clear visualization of the stent lumen. MIP, maximum intensity projection; SUMO, susceptibility gradient mapping using the original resolution; GRASP, gradient echo acquisition for super-paramagnetic particles.

to calculate the field map, which is critical for the accurate calculation of the susceptibility values. On the other hand, the stent becomes less visible when the lower spatial resolution is used because of the partial volume effect (20). Therefore, based upon our experience, the best visualization is obtained at the resolution of 0.7 mm on most stents.

Although the stent is well identified and visualized from the gel phantom in the second experiment, it is not well differentiated from the background in the third experiment. The reason is due to different phantoms were used in the second and the third experiments. In addition, a pump is used in the third experiment to simulate blood flow within the stent, which can influence the susceptibility quantification. Nevertheless, the phantom is used for evaluating the stent restenosis, which had been carefully designed according to previous work (22). Experiment results show that the stenosis is easily identified by the susceptibility-based method rather than the SUMO and GRASP. Furthermore, SUMO and GRASP imaged the surrounding area of the stent rather than its precise location (see *Figure 7B,C,E,F*). In contrast, the susceptibility-based method can localize the real location of the stent compared

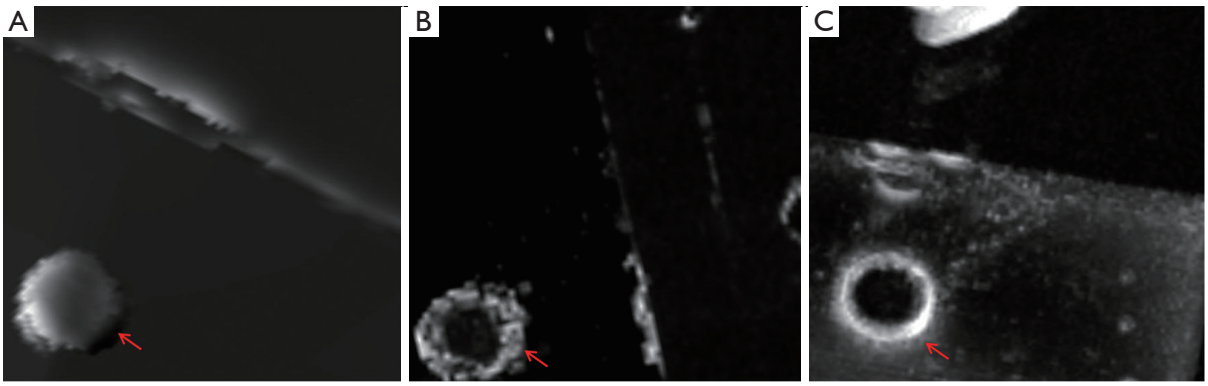

Figure 14 MIP reconstructions of the stent with external stenosis (A) the susceptibility-based method, (B) SUMO, and (C) GRASP. The susceptibility-based method and the GRASP can provide a clear visualization of the stent lumen. The red arrows indicate the external stenosis. MIP, maximum intensity projection; SUMO, susceptibility gradient mapping using the original resolution; GRASP, gradient echo acquisition for super-paramagnetic particles.

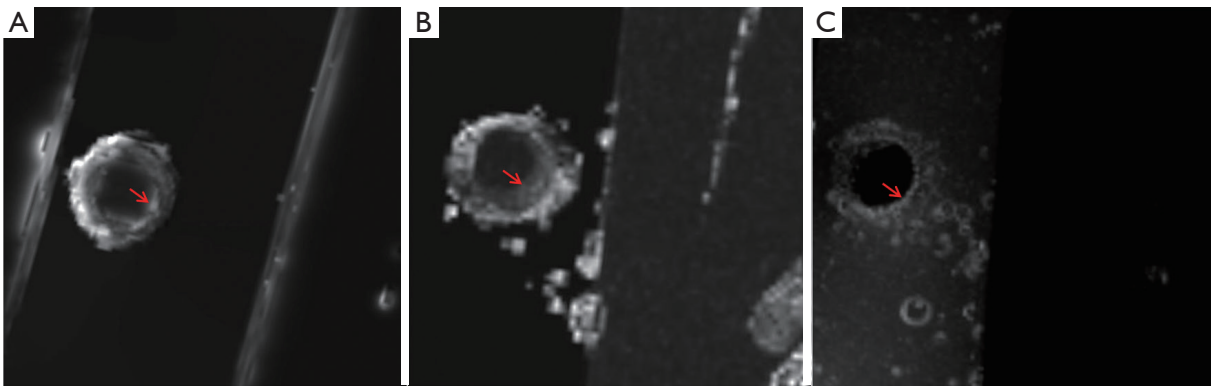

Figure 15 MIP reconstructions of the stent with internal stenosis (A) the susceptibility-based method, (B) SUMO, and (C) GRASP. The susceptibility-based method and the SUMO can provide a clear visualization of the stent lumen. The red arrows indicate the external stenosis. MIP, maximum intensity projection; SUMO, susceptibility gradient mapping using the original resolution; GRASP, gradient echo acquisition for super-paramagnetic particles.

to SUMO and GRASP methods (see *Figure 7A,D*). This comparison had been evaluated by using a gel phantom in the second experiment. Both good soft-tissue contrast and accurate stent localization could be achieved simultaneously by combining the conventional images with the positive contrast images obtained using the susceptibility-based imaging method. It is of note that the susceptibility-based method has severe RF shield artifacts because of the extended data sampling time and the high RF excitation time. Nevertheless, the susceptibility-based method still shows superior performance for the visualization and localization of the implanted stent.

There are several limitations to this study. First, the experiments are only performed with phantoms which may be very different from the *in vivo* study. Efforts to make the model as close to the *in vivo* situation as possible would help reduce this gap. Second, we do not perform exact physical measurements of the luminal diameters in the quantitative assessment of the stenosis because of the distortion of the material during extraction and postprocessing of the stents. Thus, the stent configuration cannot be preserved introducing some measurement bias. Third, various levels of stenosis and fractures are not tested which would be key areas of investigation for subsequent studies. Fourth, the stent is positioned parallel to the main field B_0 in the experiment. Since the direction of the stent is random

in vivo, this setting does not reflect the real situation. In the future, a targeted *in vivo* study that builds on the results of this work would be highly beneficial.

Conclusions

The susceptibility-based method can be used to localize the position of the stent and to identify the stent restenosis when optimal stent orientation and resolution are used. The technique has the potential to become a non-invasive imaging tool for post-angioplasty and stent surgery evaluation.

Acknowledgements

Funding: This work was supported in part by the International Cooperation and Exchange of the National Science Foundation of China (81729003), National Key Research and Development Program of China (2016YFC0100302), the National Natural Science Foundation of China (81571669, 61201442, 61471350, 81729003), the Natural Science Foundation of Shenzhen (JCYJ20160531174850658, GJHZ20150316143320494, KQCX2015033117354154, JCYJ20160331185933583, JCYJ20150831154213680), the Natural Science Foundation of Guangdong Province (2014A030312006, 2014B030301013), the Medical Scientific Research Foundation of Guangdong Province, China (20161139128243), the Guangdong Provincial Key Laboratory of Medical Image Processing (2014B030301042, 2017A050501026) and the Strategic Priority Research Program of Chinese Academy of Sciences (XDB25000000). The authors should also thank a lot for the supports from the National Natural Science Foundation of China (61871373), Natural Science Foundation of Guangdong Province (2018A0303130132), Shenzhen Key Laboratory of Ultrasound Imaging and Therapy (ZDSYS20180206180631473).

Footnote

Conflicts of Interest: The authors have no conflicts of interest to declare.

Ethical Statement: All experiments were conducted *in vitro* model and all the experimental procedures were conducted with strict adherence to the guidelines by the Animal Ethics Committee.

References

1. Lammer J, Bosiers M, Zeller T, Schillinger M, Boone E, Zaugg MJ, Verta P, Peng L, Gao X, Schwartz LB. First clinical trial of nitinol self-expanding everolimus-eluting stent implantation for peripheral arterial occlusive disease. J Vasc Surg 2011;54:394-401.
2. Bean MJ, Johnson PT, Roseborough GS, Black JH, Fishman EK. Thoracic Aortic Stent-Grafts: Utility of Multidetector CT for Pre- and Postprocedure Evaluation. Radiographics 2008;28:1835-51.
3. Sun Z, Ng CKC, Sá Dos Reis C. Synchrotron radiation computed tomography versus conventional computed tomography for assessment of four types of stent grafts used for endovascular treatment of thoracic and abdominal aortic aneurysms. Quant Imaging Med Surg 2018;8:609-20.
4. Almutairi A, Al Safran Z, AlZaabi SA, Sun ZH. Dual energy CT angiography in peripheral arterial stents: optimal scanning protocols with regard to image quality and radiation dose. Quant Imaging Med Surg 2017;7:520-31.
5. Fazel R, Krumholz HM, Wang Y, Ross JS, Chen J, Ting HH, Shah ND, Nasir K, Einstein AJ, Nallamothu BK. Exposure to Low-Dose Ionizing Radiation from Medical Imaging Procedures. New Engl J Med 2009;361:849-57.
6. Sodickson A, Baeyens PF, Andriole KP, Prevedello LM, Nawfel RD, Hanson R, Khorasani R. Recurrent CT, Cumulative Radiation Exposure, and Associated Radiation-induced Cancer Risks from CT of Adults. Radiology 2009;251:175-84.
7. Roach M, Faillace-Akazawa P, Malfatti C, Holland J, Hricak H. Prostate volumes defined by magnetic resonance imaging and computerized tomographic scans for three-dimensional conformal radiotherapy. Int J Radiat Oncol Biol Phys 1996;35:1011-8.
8. Griffey RT, Sodickson A. Cumulative Radiation Exposure and Cancer Risk Estimates in Emergency Department Patients Undergoing Repeat or Multiple CT. AJR Am J Roentgenol 2009;192:887-92.
9. Syha R, Ketelsen D, Kaempf M, Mangold S, Sixt S, Zeller T, Springer F, Schick F, Claussen CD, Brechtel K. In vitro stent lumen visualisation of various common and newly developed femoral artery stents using MR angiography at 1.5 and 3 tesla. Eur Radiol 2013;23:588-95.
10. Chiang CH, Tseng YC, Chen AC, Huang YL, Chen DYT, Chen CJ, Lin YK, Hsu HL. In vitro comparison of intracranial stent visibility using various concentrations of gadolinium contrast agent under 1.5 T and 3 T MR

angiography. J Neurointerv Surg 2017;9:399-404.
11. Hickethier T, Kröger JR, Von Spiczak J, Baessler B, Pfister R, Maintz D, Bunck AC, Michels G. Non-invasive imaging of bioresorbable coronary scaffolds using CT and MRI: First in vitro experience. Int J Cardiol 2016;206:101-6.
12. Gitsioudis G, Fortner P, Stuber M, Missiou A, Andre F, Muller OJ, Katus HA, Korosoglou G. Off-resonance magnetic resonance angiography improves visualization of in-stent lumen in peripheral nitinol stents compared to conventional T1-weighted acquisitions: an in vitro comparison study. Int J Cardiovasc Imaging 2016;32:1645-55.
13. Hilliard NJ, Hayes P, Winterbottom AP. Appearance of the Nellix endoprosthesis on postoperative imaging: implications for patient and device surveillance. Semin Vasc Surg 2016;29:126-34.
14. Mani V, Briley-Saebo K, Hyafil F, Itskovich V, Fayad Z. Positive magnetic resonance signal enhancement from ferritin using a GRASP (GRE acquisition for superparamagnetic particles) sequence: ex vivo and in vivo study. J Cardiovasc Magn Reson 2006;8:49-50.
15. Mani V, Briley-Saebo KC, Itskovich VV, Samber DD, Fayad ZA. Gradient echo acquisition for superparamagnetic particles with positive contrast (GRASP): sequence characterization in membrane and glass superparamagnetic iron oxide phantoms at 1.5T and 3T. Magn Reson Med 2006;55:126-35.
16. Dahnke H, Liu W, Herzka D, Frank JA, Schaeffter T. Susceptibility gradient mapping (SGM): a new postprocessing method for positive contrast generation applied to superparamagnetic iron oxide particle (SPIO)-labeled cells. Magn Reson Med 2008;60:595-603.
17. Varma G, Clough RE, Acher P, Senegas J, Dahnke H, Keevil SF, Schaeffter T. Positive visualization of implanted devices with susceptibility gradient mapping using the original resolution. Magn Reson Med 2011;65:1483-90.
18. Vonken EJ, Schar M, Stuber M. Positive contrast visualization of nitinol devices using susceptibility gradient mapping. Magn Reson Med 2008;60:588-94.
19. Varma G, Clough R, Sénégas J, Keevil SF, Schaeffter T. Positive visualization of nitinol stent-grafts by post-processing. J Cardiovasc Magn Reson 2010;12:1-2.
20. Dong Y, Chang Z, Xie G, Whitehead G, Ji JX. Susceptibility-based positive contrast MRI of brachytherapy seeds. Magn Reson Med 2015;74:716-26.
21. Shi C, Xie G, Zhang Y, Zhang X, Chen M, Su S, Dong Y, Liu X, Ji J. Accelerated susceptibility-based positive contrast imaging of MR compatible metallic devices based on modified fast spin echo sequences. Phys Med Biol 2017;62:2505-20.
22. Nordmeyer J, Gaudin R, Tann OR, Lurz PC, Bonhoeffer P, Taylor AM, Muthurangu V. MRI may be sufficient for noninvasive assessment of great vessel stents: an in vitro comparison of MRI, CT, and conventional angiography. AJR Am J Roentgenol 2010;195:865-71.
23. Muthurangu V, Taylor A, Andriantsimiavona R, Hegde S, Miquel ME, Tulloh R, Baker E, Hill DL, Razavi RS. Novel method of quantifying pulmonary vascular resistance by use of simultaneous invasive pressure monitoring and phase-contrast magnetic resonance flow. Circulation 2004;110:826-34.
24. Whitehead G, Ji J. Positive contrast MRI of prostate brachytherapy seeds based on resonant frequency offset mapping. Conf Proc IEEE Eng Med Biol Soc 2010;2010:6641-4.
25. Bartels LW, Bakker CJG, Viergever MA. Improved lumen visualization in metallic vascular implants by reducing RF artifacts. Magn Reson Med 2002;47:171-80.

Cite this article as: Shi C, Xie G, Liang D, Wang H, Huang Y, Ren Y, Xue Y, Chen H, Su S, Liu X. Positive visualization of MR-compatible nitinol stent using a susceptibility-based imaging technique. Quant Imaging Med Surg 2019;9(3):477-490. doi: 10.21037/qims.2019.03.15

